

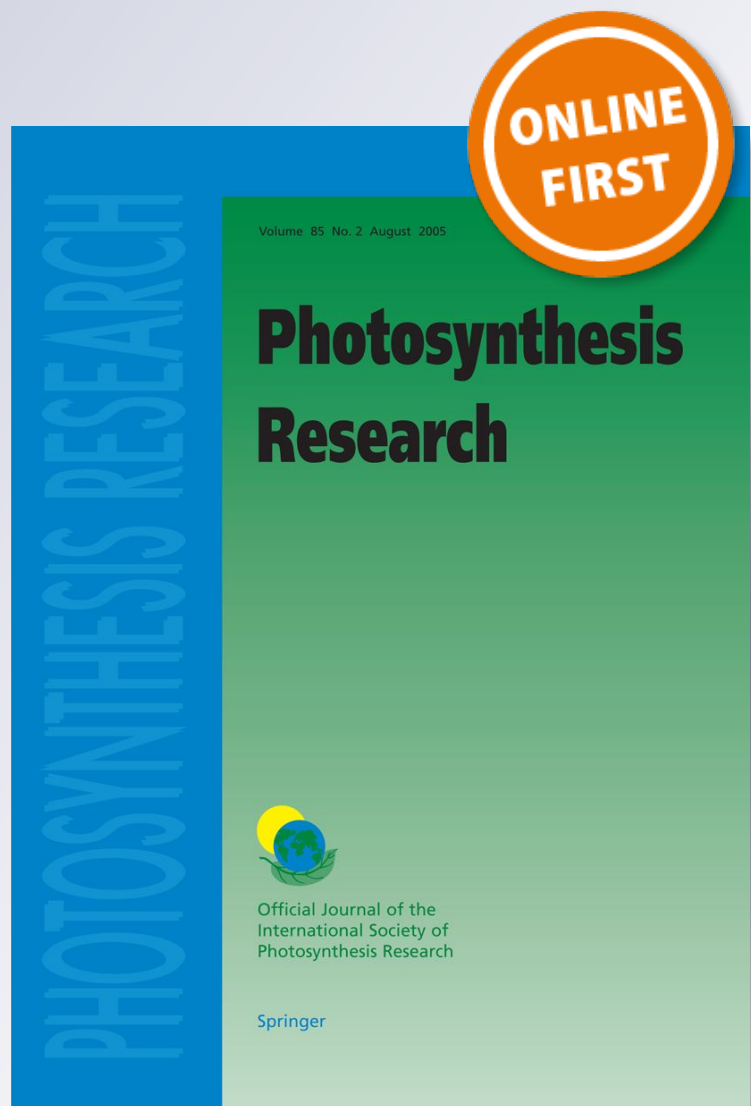
Electron requirements for carbon incorporation along a diel light cycle in three marine diatom species

Jérôme Morelle & Pascal Claquin

Photosynthesis Research
Official Journal of the International
Society of Photosynthesis Research

ISSN 0166-8595

Photosynth Res
DOI 10.1007/s11120-018-0491-2



Your article is protected by copyright and all rights are held exclusively by Springer Science+Business Media B.V., part of Springer Nature. This e-offprint is for personal use only and shall not be self-archived in electronic repositories. If you wish to self-archive your article, please use the accepted manuscript version for posting on your own website. You may further deposit the accepted manuscript version in any repository, provided it is only made publicly available 12 months after official publication or later and provided acknowledgement is given to the original source of publication and a link is inserted to the published article on Springer's website. The link must be accompanied by the following text: "The final publication is available at link.springer.com".



Electron requirements for carbon incorporation along a diel light cycle in three marine diatom species

Jérôme Morelle^{1,2} · Pascal Claquin^{1,2} Received: 21 July 2017 / Accepted: 18 February 2018
© Springer Science+Business Media B.V., part of Springer Nature 2018

Abstract

Diatoms account for about 40% of primary production in highly productive ecosystems. The development of a new generation of fluorometers has made it possible to improve estimation of the electron transport rate from photosystem II, which, when coupled with the carbon incorporation rate enables estimation of the electrons required for carbon fixation. The aim of this study was to investigate the daily dynamics of these electron requirements as a function of the diel light cycle in three relevant diatom species and to apprehend if the method of estimating the electron transport rate can lead to different pictures of the dynamics. The results confirmed the species-dependent capacity for photoacclimation under increasing light levels. Despite daily variations in the photosynthetic parameters, the results of this study underline the low daily variability of the electron requirements estimated using functional absorption of the photosystem II compared to an estimation based on a specific absorption cross section of chlorophyll *a*. The stability of the electron requirements throughout the day would suggest it is potentially possible to estimate high-frequency primary production by using autonomous variable fluorescence measurements from ships-of-opportunity or moorings, without taking potential daily variation in this parameter into consideration, but this result has to be confirmed on natural phytoplankton assemblages. The results obtained in this study confirm the low electron requirements of diatoms to perform photosynthesis, and suggest a potential additional source of energy for carbon fixation, as recently described in the literature for this class.

Keywords Phytoplankton · Photosynthesis · PAM · ¹³C incorporation · Electron transport rate (ETR)

Introduction

Because primary production sustains each group in the marine food web (Pauly and Christensen 1995), accurate estimation of its short-term dynamics is a key to capturing, understanding, and managing marine ecosystems (Cloern et al. 2014). The main method traditionally used to estimate primary production is carbon (¹³C or ¹⁴C) incorporation (Babin et al. 1994; Cloern et al. 2014). The disadvantage of this method is the long incubation time, which prevents the estimation of high-frequency primary production at spatial

and temporal scales. An alternative rapid and automatic way of obtaining high-frequency measurements is fluorometry, which is based on variations in the fluorescence of photosystem II (PSII). This flexible, sensitive, and non-invasive method (Kromkamp and Forster 2003) enables access to the photosynthetic rate but not to production in terms of fixed carbon (Kolber and Falkowski 1993; Barranguet and Kromkamp 2000). Two principal fluorescence-based methods are currently used, the single-turnover method (ST) and the multi-turnover method (MT) (Kromkamp and Forster 2003). The ST method progressively reduces the first stable acceptor, Q_A . This method makes it possible to calculate the functional absorption of the PSII (σ_{PSII}) and to determine a fluorescence-based photosynthetic rate that can be used to estimate a fluorescence-based carbon fixation rate (Kolber and Falkowski 1993). The MT method classically used in pulse amplitude modulated (PAM) fluorometry can reduce the total set of electron acceptors. When combined with estimation of the specific absorption of the chlorophyll pigment (a^*), the MT method enabled estimation of the

✉ Pascal Claquin
pascal.claquin@unicaen.fr

¹ Normandie Université, Université de Caen -Normandie, 14032 Caen, France

² UMR BOREA, Muséum National d'Histoire Naturelle, CNRS-7208, IRD-207, Sorbonne Université, Université Caen-Normandie, Université des Antilles, Esplanade de la paix, 14032 Caen, France

electron transport rate (ETR) (Barranguet and Kromkamp 2000; Napoléon and Claquin 2012). The development of new generations of fluorometers makes it possible to merge some of the advantages of the two fluorescence methods and to refine and improve the estimation of the ETR (Schreiber et al. 2012). In order to calculate high-frequency carbon incorporation, the ETR values can be plotted against the carbon incorporation rate determined using $^{13/14}\text{C}$ methods to estimate the electrons needed to fix a mole of carbon ($\varphi_{e,C}$) (Kolber and Falkowski 1993; Barranguet and Kromkamp 2000; Kromkamp and Forster 2003; Juneau and Harrison 2005; Marchetti et al. 2006; Hancke et al. 2008b, 2015; Napoléon and Claquin 2012; Napoléon et al. 2013a; Zhu et al. 2016; Schuback et al. 2017). However, this parameter does not remain spatially and temporally constant due to the many physical, chemical, and biological factor that influence both carbon fixation and electron fluxes, for example, temperature (Morris and Kromkamp 2003), concentration of nutrients (Napoléon et al. 2013b), or species composition (Behrenfeld et al. 2004). However, the main parameter that influences primary production is the irradiance level. There are many different time scales of variations in light intensities ranging from variations due to waves at the air–water interface to variations in the light regime at seasonal scale. The most important level of variation in irradiance is the light–dark rhythm (Falkowski 1984), which strongly influences daily primary production rates. The diel variations in primary production can generally be explained by the circadian rhythms (Prézelin 1992) and species composition (Litchman 1998; Huisman et al. 2004). However, at a high level of irradiance, photoacclimation has been shown to be the main process affecting the photosynthetic apparatus and can greatly affect the daily primary production dynamics (Macintyre et al. 2002; Behrenfeld et al. 2004; Van De Poll et al. 2009).

Although some authors have investigated ETR/C relationships and $\varphi_{e,C}$ dynamics, none have studied daily variations in $\varphi_{e,C}$ that could influence estimations of daily primary production using variable fluorescence techniques. This point is particularly important in the context of achieving independent estimations of primary production based on ETR estimation from ships-of-opportunity or moorings (Lawrenz et al. 2013; Napoléon and Claquin 2012; Silsbe et al. 2015; Houliez et al. 2017; Claquin et al. in prep). The aim of this study was to investigate the daily dynamics of ETR/C relationships and $\varphi_{e,C}$ as a function of the diel light cycle considering photosynthetic parameters dynamics in order to better understand daily variations in primary production. Furthermore, the different methods currently used to estimate ETR can influence the estimation of $\varphi_{e,C}$ (Lawrenz et al. 2013). For that reason, ETR was estimated, in this study, using two different methods based on the same rETR measurements. On the one hand using a^* (Barranguet and Kromkamp 2000;

Morris and Kromkamp 2003; Napoléon and Claquin 2012; Napoléon et al. 2013b), and on the other hand, using σ_{PSII} (Schreiber et al. 2012). In addition to comparing the two methods of estimation, our aim was to understand if the methods produce different pictures of $\varphi_{e,C}$ daily dynamics. The study was conducted on three species belonging to the same phylum, the diatom species (Bacillariophyceae), which is one of the most important groups of primary producers (Armbrust 2009) in marine ecosystems (Nelson et al. 1995; Geider et al. 2001) and which plays a major role in exporting organic carbon (Buesseler 1998; Ducklow et al. 2001; Henson et al. 2012).

Methods

Culture conditions

Three cosmopolitan marine diatom species (Bacillariophyceae) were investigated in this study: two centric diatoms, *Thalassiosira pseudonana* (Hasle and Heimdal, CCMP H1), which is a model for diatom physiology studies, *Skeletonema marinoi* (Sarno & Zingone, isolated in the English Channel), which is particularly abundant during spring blooms, and the pennate diatom *Pseudo-nitzschia australis* (Frenguelli, isolated in the English Channel), which produces “Domoic acid,” which is responsible for amnesic shellfish poisoning (Thorel et al. 2014).

For each species, semi-continuous cultures (2.5 l) were performed in triplicate in sterile 4 l Pyrex flasks using autoclaved and filtered natural poor seawater enriched in nutrients with f/2-medium (Guillard and Ryther 1962). The cultures were maintained in an incubator (Snijders Scientific, Netherlands) at 18 °C with a step-by-step sinusoidal light intensity cycle and a 12:12 h light/dark photoperiod. The light intensity, provided by daylight fluorescent lamps, was varied step by step from 0 to 175 $\mu\text{mol photons m}^{-2} \text{s}^{-1}$ at 2 pm which mimic the variation of the integrated light in coastal English Channel (Seine Bay, SOMLIT data, Lucsur-mer, France).

Each day of culture growth, cultures were manually mixed by gentle swirling every 4 h during the light cycle and the integrity of the cells was checked under the microscope. Biomass was estimated by in vivo *chl a* measurements using a turner TD-700 fluorometer (Turner Designs, California USA) and dilutions were performed to maintain maximum exponential growth. Experiments were started when the cells kept their growth rate constant for 5 consecutive days (Claquin et al. 2008). During experiments, chlorophyll *a* (*chl a*) concentrations, chlorophyll-specific absorption cross sections (a^* and σ_{PSII440}), and photosynthetic parameters were measured at hourly intervals during the light cycle and ^{13}C incubation experiments were performed three times a

day: 8:30 am, 2 pm, and 7:30 pm (i.e., 0.5, 6, and 11.5 h, respectively, after experimental dawn).

Chlorophyll parameters

To measure the chl *a* concentration, at each hour of the experiments, 10 mL of each culture was centrifuged for 10 min at 4000 rpm. Pigments were extracted by adding 90% acetone (v/v) to the pellet, which was stored for 12 h in the dark at 4 °C. After centrifugation at 4000 rpm for 5 min at 4 °C, the concentration of chl *a* was measured in the supernatant using a Turner TD-700 fluorometer (Turner Designs, Sunnyvale, California, USA) and is expressed in $\mu\text{g L}^{-1}$ (Welschmeyer 1994).

The chlorophyll-specific absorption cross section (a^* ; $\text{m}^2 \text{mgChl } a^{-1}$) was obtained by measuring the in vivo optical density of the cultures in a spectrophotometer (Ultraspec 1000) using Shibata method (Shibata et al. 1954). The a^* was calculated using the average optical density between 400 and 700 nm ($A_{400-700}$) and the concentration of chl *a* (mg m^{-3}), according to the equation of Dubinsky et al. (1986) specific to concentrated suspension cultures:

$$a^* = \frac{A \times 100 \times \ln(10)}{[\text{Chl } a]} \quad (1)$$

Photosynthesis and primary production measurements

^{13}C incubation

For each replication and three times a day, a volume of 650 ml was inoculated with $\text{NaH}^{13}\text{CO}_3$ (98 atom %, Sigma-Aldrich) corresponding to 15% enrichment of the dissolved inorganic carbon present. The homogenized enrichment was shared between ten 62-ml culture flasks including a dark flask used to estimate incorporation of non-photosynthetic carbon. All the flasks were placed in line inside a photosynthetron [modified from Babin et al. (1994)] maintained at 18 °C by a water circuit and illuminated by a U-shaped dimmable fluorescent tube (OSRAM, DULUX L, 2G11, 55W/12–950, daylight). Each 62-ml flask was then illuminated with constant light for 90 min before collection. The light intensity in each flask was measured using a microspherical quantum sensor (US-SQS; Walz) connected to a LI-COR 1400 data logger. Irradiance (*E*) varied from one flask to another with values of 0, 24, 36, 54, 80, 122, 285, 426, 608, and 848 $\mu\text{mol photons m}^{-2} \text{s}^{-1}$, respectively. After incubation, each flask was filtered on GF/F filters (pre-combusted at 450 °C for 4 h) and stored at –20 °C until analysis. Before analyses, filters were exposed to fuming HCL for 4 h and dried at 50 °C for 12 h to remove carbohydrates. After

being placed in tin capsules, the samples were conserved at 50 °C until measurement.

The isotopic ratio of ^{13}C to ^{12}C and the concentration of particulate organic carbon (POC) were determined using an EA 300 elemental analyzer (Eutovector, Milan, Italy) combined with a mass spectrophotometer (IsoPrime, Elementar). After the dark incorporation value was subtracted, the carbon fixation rates (P^{chl} ; $\text{mmolC mgchl } a^{-1} \text{ h}^{-1}$) were calculated according to Hama et al. (1983).

The $P^{\text{chl}}(E)$ values were plotted against the irradiance values (*E*) applied during the experiment to generate PE curves (see below).

Multi-color-PAM fluorometry

The Multi-Color-PAM fluorometer (Walz, Effeltrich, Germany; Schreiber et al. 2012) makes it possible to analyze the kinetics of the O–I₁ fluorescence rise at 440 nm by using the fitting routine of the PamWin-3 program based on the reversible radical pair model of PSII of Lavergne and Trissl (1995) extended to account for Q_A -re-oxidation (Schreiber et al. 2012). This ST method enables estimation of the constant time of Q_A -reduction during the O–I₁ rise (τ ; ms) and calculation of the functional absorption of the PSII (σ_{PSII440} ; nm^2) as follows:

$$\sigma_{\text{PSII440}} = \frac{1}{\tau \times L \times I} \quad (2)$$

where *L* is Avogadro's constant and *I* is the photon fluence rate of the light driving the O–I₁ rise (*E*; $\mu\text{mol quanta m}^{-2} \text{s}^{-1}$). The σ_{PSII440} values were then calculated on a 3 ml not-concentrated sub-sample at each hour of the experiments.

The Multi-Color-PAM device also enables estimation of the maximum energy conversion efficiency or quantum efficiency of PSII charge separation ($Y(\text{II})_{\text{max}}$: fluorescence ratio). After 10 min of dark acclimation to allow oxidation of the electron acceptor pool, a second 3 ml not-concentrated sub-sample was transferred into the measuring chamber. The sample was excited by a low-frequency measuring light ($1 \mu\text{mol photons m}^{-2} \text{s}^{-1}$; $\lambda = 440 \text{ nm}$) to access the quasi-dark level of fluorescence yield (F_0). After a saturating light pulse ($2500 \mu\text{mol photons m}^{-2} \text{s}^{-1}$; $\lambda = 440 \text{ nm}$), making it possible to reduce the pools of Quinone A (Q_A), Quinone B (Q_B), and part of the plastoquinone (PQ), the maximum fluorescence (F_M) was obtained. After subtraction of the blank fluorescence measured on culture medium filtered through a GF/F glass-fiber filter, $Y(\text{II})_{\text{max}}$ was calculated at each hour of the experiments according to the following equation (Schreiber et al. 2012):

$$Y(\text{II})_{\text{max}} = \frac{F_V}{F_M} = \frac{F_M - F_0}{F_M} \quad (3)$$

In accordance with Eq. 3, $Y(II)_{\max}$ variations are due to F_0 and/or F_M dynamics. However, the level of F_0 and F_M can depend on *chl a* concentration or/and on $\sigma_{PSII440}$ dynamics (Oxborough et al. 2012). In order to identify the implication of these parameters in $Y(II)_{\max}$ variations, the values of F_0 and F_M were divided by the concentration of *chl a* and the $\sigma_{PSII440}$:

$$\frac{F_0 \text{ (or } F_M)}{[Chl a]} \quad (4)$$

$$\frac{F_0 \text{ (or } F_M)}{[Chl a] \times \sigma_{PSII440}} \quad (5)$$

After $Y(II)_{\max}$ was estimated and independently from Eqs. 4, 5, the samples were exposed to 14 increasing levels of blue light (E ; $\lambda=440$ nm) from 0 to 966 $\mu\text{mol photons m}^{-2} \text{s}^{-1}$ with 55 s at each step ($E=0$; 12; 23; 24; 48; 77; 109; 158; 224; 309; 445; 598; 766; 966 $\mu\text{mol photons.m}^{-2} \text{s}^{-1}$). At each level of light, a steady-state fluorescence (F_S) and a maximum fluorescence (F_M') were measured and $Y(II)$ for each irradiance was determined using Eq. 6 (Schreiber et al. 2012). Subsequently, the relative electron transport rate (rETR; $\mu\text{mol m}^{-2} \text{s}^{-1}$) which represents the rate of linear electron transport through PSII and is correlated with the overall photosynthetic performance of the phytoplankton (Juneau and Harrison 2005) was calculated for each irradiance following Eq. 7:

$$Y(II) = \frac{F_M' - F_S}{F_M'} \quad (6)$$

$$rETR(E) = Y(II) \times E. \quad (7)$$

Calculation of the electron transport rate

Two methods of calculation were used to estimate the absolute ETR from PSII. Firstly, the ETR ($\text{mmol}^{-1} \text{mgchl a}^{-1} \text{h}^{-1}$) was estimated using the a^* ($\text{m}^2 \text{mgChl a}^{-1}$) values (Gilbert et al. 2000; Napoléon et al. 2013a) following Eq. 8 and called ETR^{a^*} .

$$ETR^{a^*}(E) = rETR(E) \times a^* \times fAQ_{PSII} \times 3.6, \quad (8)$$

where fAQ_{PSII} is the fraction of absorbed quanta to PSII assuming that, for diatoms, 74% of the absorbed photons were allocated to photoreactions in the PSII (Johnsen and Sakshaug 2007; Napoléon et al. 2013a). Secondly, the ETR was estimated using the $\sigma_{PSII440}$ values (nm^2) following Eq. 9, named $ETR(II)$, and was converted in $\text{mmol}^{-1} \text{mgchl a}^{-1} \text{h}^{-1}$ according to Schreiber et al. (2012).

$$ETR(II) = \frac{rETR(E) \times \sigma_{PSII}}{Y(II)_{\max}} \times \frac{[PSII] \times 36.10^5}{[chl a]}, \quad (9)$$

where $[chl a]$ is the *chl a* concentration expressed in mg ml^{-1} and $[PSII]$ is the concentration of the PSII reaction centers in PSII ml^{-1} obtained as follows:

$$[PSII] = \frac{[chl a] \times L}{900 \times 1000}, \quad (10)$$

where $[chl a]$ is expressed in g ml^{-1} assuming a molecular weight of 900 g mol^{-1} per chl and a photosynthetic unit size of 1000 molecules of chl per electron transport chain as described by Schreiber et al. (2012).

PE curves

The $P^{chl}(E)$, $ETR^{a^*}(E)$, and $ETR(II)(E)$ values were, respectively, plotted against the irradiance (E) applied during each respective measurements. The mechanistic model of Eilers and Peeters (1988) (Eq. 8) was used to fit the data using SigmaPlot 11.0 (Systat Software Inc. Chicago, USA) and to extract the equation coefficients (a , b , and c) in order to calculate the maximum photosynthetic capacity (P^{chl}_{\max} , $ETR^{a^*}_{\max}$, and $ETR(II)_{\max}$; Eq. 9) and the photosynthetic efficiency for ETR^{a^*} (α^*) and $ETR(II)$ ($\alpha(II)$) in ($\text{mmol mgchl a}^{-1} \text{h}^{-1}$).($\mu\text{mol photons m}^{-2} \text{s}^{-1}$) $^{-1}$; (Eq. 10):

$$X(E) = \frac{E}{aE^2 + bE + c} \quad (11)$$

$$X_{\max} = \frac{1}{(b + 2\sqrt{ac})} \quad (12)$$

$$\alpha = \frac{1}{c}. \quad (13)$$

The $ETR^{a^*}_{\max}$ and $ETR(II)_{\max}$ values were plotted against each other in order to compared the two way of calculation.

Electrons required for C fixation ($\varphi_{e,C}$)

The model of the PE curves obtained from P^{chl} and each ETR ($ETR(II)$ and ETR^{a^*}) was used to calculated new values using the same irradiance level for all parameters ($E=0$; 24; 36; 54; 80; 122; 285; 426; 608; 848 $\mu\text{mol photons m}^{-2} \text{s}^{-1}$). These values were plotted against each other in order to calculate $\varphi_{e,C}$ which corresponds to the initial slope of the relationship between P^{chl} and ETR (Barranguet and Kromkamp 2000; Napoléon et al. 2013b). $\varphi_{e,C}$ was calculated for each species in the triplicate cultures, at the three different times during the light period. Because $ETR(II)$ was estimated by using $\sigma_{PSII440}$ and ^{13}C incorporation using white light, a spectral correction was performed by using the $a^*_{440}:a^*$ ratio (Suggett et al. 2004; Lawrenz et al. 2013). Therefore, three

$\varphi_{e,C}$ values were calculated, $\varphi_{e,C}^{a^*}$, $\varphi_{e,C}^{\sigma}$ (not corrected), $\varphi_{e,C}^{\sigma}$ (corrected).

Data analyses

In order to investigate the significant effect of the diel cycle on biological (a^* , chl_a) and photosynthetic ($Y(II)_{max}$, σ_{PSII} , $ETR_{max}^{a^*}$, $ETR(II)_{max}$, P^{Chl}_{max} , $\varphi_{e,C}$) parameters, repeated measures analysis of variance (RM ANOVA) were performed followed by Holm–Sidak pairwise comparison tests using SigmaPlot 11.0 (Systat Software). Previously, the presence of outliers, non-normality of residuals, and the lack of homoscedasticity were tested using Shapiro and Bartlett tests, respectively. Differences were considered significant when the p value was less than 0.05. All plots were performed using SigmaPlot 11.0 (Systat Software). Linear regressions and Spearman correlations were also performed on plots.

Results

Chla and absorption cross section

Chl_a concentrations showed significant increasing trends as the sampling day advanced with values ranging from 133.4 to 238.8 $\mu g L^{-1}$ for *T. pseudonana*, from 261.2 to 347.1 $\mu g L^{-1}$ for *S. marinoi*, and from 43.1 to 55.3 $\mu g L^{-1}$ for *P. australis* which is in accordance with the growth stage of the cultures. The values of a^* (Fig. 1a) decreased as the day advanced from 0.013 to 0.004 $m^2 mgchl_a^{-1}$ for *T. pseudonana*, from 0.038 to 0.030 $m^2 mgchl_a^{-1}$ for *P. australis*, and remained almost constant for *S. marinoi* at

$0.007 \pm 0.0006 m^2 mgchl_a^{-1}$. The $\sigma_{PSII440}$ (Fig. 1b) showed no significant differences over the course of the day for *T. pseudonana* with a daily mean value of $2.98 \pm 0.28 nm^2$. For *S. marinoi*, the lowest value ($1.71 \pm 0.20 nm^2$) recorded at 2 pm differed significantly from the other values recorded during the day (in mean $2.44 \pm 0.17 nm^2$). For *P. australis*, values ranged between 2.64 ± 0.55 and $4.16 \pm 1.05 nm^2$ but due to the high variability between replicates, no significant differences were recorded (RM ANOVA, $p=0.185$).

Quantum efficiency of PSII charge separation

$Y(II)_{max}$ (Fig. 2) showed high values ranging between 0.621 and 0.668 for *T. pseudonana*, between 0.502 and 0.636 for *S. marinoi*, and between 0.652 and 0.680 for *P. australis*. For *T. pseudonana*, values after 2 pm were significantly lower than values before. For *S. marinoi*, a significant decrease was measured from 11:30 am to 2 pm followed by a significant increase from 2 pm to 4:30 pm. For *P. australis*, despite a low variability, values increased significantly in the morning from 7:30 am to 12:30 pm, decreased significantly between 12:30 pm and 2 pm, and no differences were recorded between 2:00 pm and 8:30 pm.

The dynamics of F_M and F_0 were investigated in order to explain the variations in $Y(II)_{max}$ (Eqs. 4, 5). For *T. pseudonana*, the significant decrease observed in $Y(II)_{max}$ at 2:00 pm was also observed for $(F_0 \text{ (or } F_M))/chl_a$ and for $(F_0 \text{ (or } F_M))/(chl_a \sigma_{PSII440})$ (Fig. 2a, b) but the variation in F_M (Fig. 2b) was greater. Thus, the $Y(II)_{max}$ can be attributed to a marked decrease in F_M independently of chl_a or $\sigma_{PSII440}$. For *S. marinoi*, the significant lowest value of $Y(II)_{max}$ observed at 2 pm was also observed for F_M/chl_a but not for $F_M/(chl_a \sigma_{PSII440})$ (Fig. 2d). This

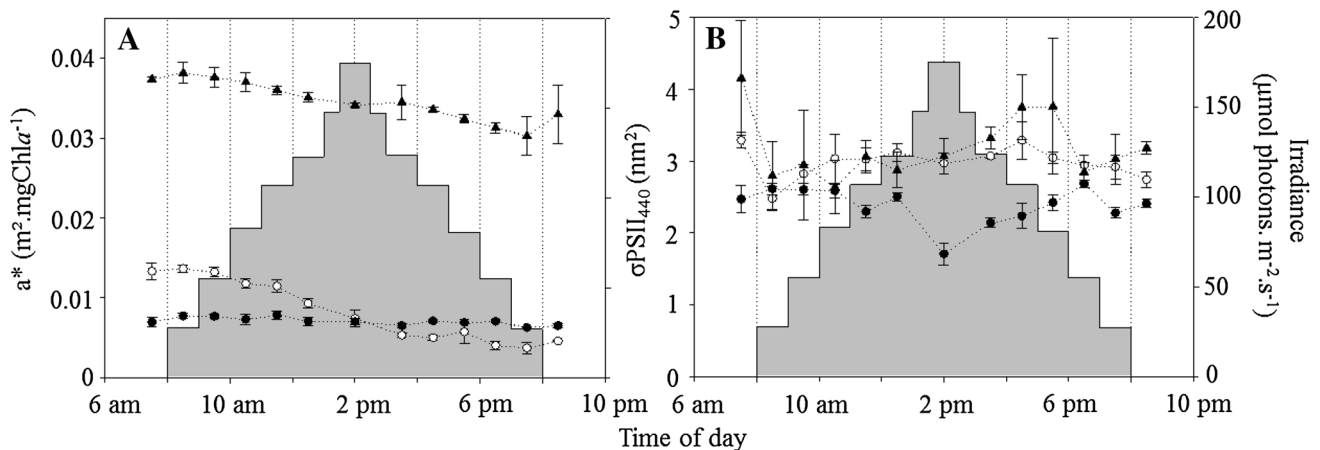


Fig. 1 Daily dynamics of **a** specific absorption of the chlorophyll pigment (a^* ; $m^2 mgChl_a^{-1}$) and **b** functional absorption cross section of the PSII (σ_{PSII} , nm^2) in the three species studied. The white circles represent *T. pseudonana*, the black circles represent *S. marinoi*, and

the black triangles represent *P. australis*. The gray bar plot represents irradiance dynamics ($\mu mol photons m^{-2} s^{-1}$) over the course of the day (times)

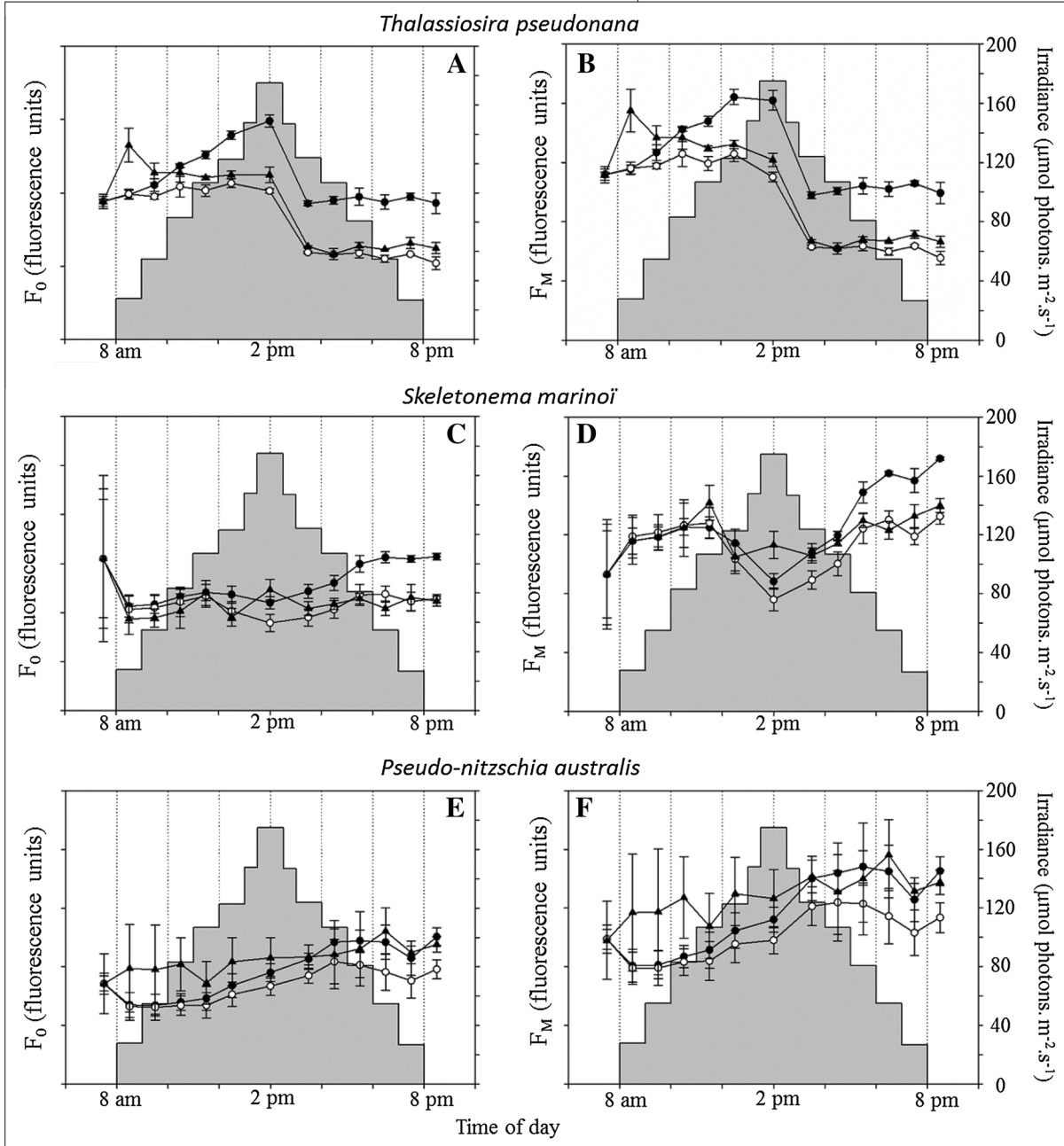
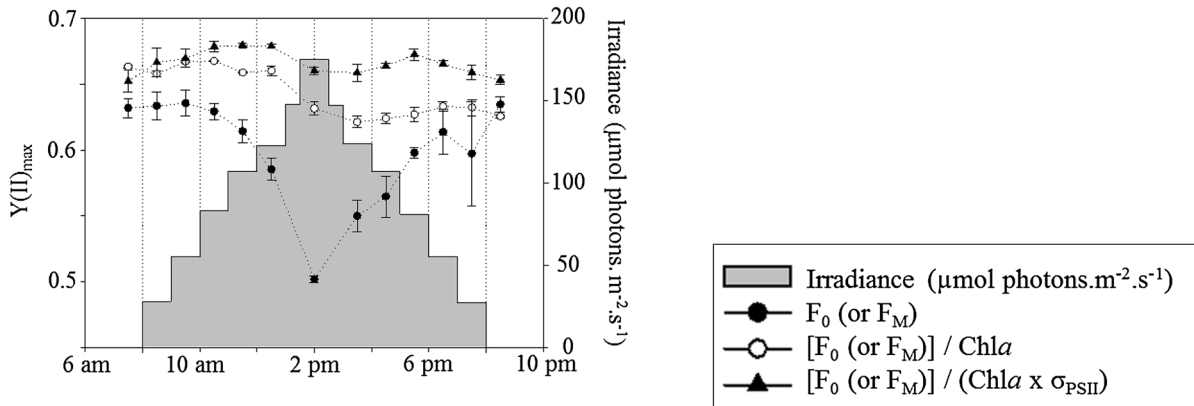


Fig. 2 Dynamics of $Y(II)_{\max}$ (fluorescence ratio), F_M (right panel) and F_0 (left panel), $F/chla$, and $F/(chla \sigma_{PSII440})$ for each studied species studied: *T. pseudonana* (a, b), *S. marinoi* (c, d), and *P. australis* (e, f). The black circles represent raw F_M and F_0 data; the empty circles represent $F_M/chla$ and $F_0/chla$ data; and the black triangles represent the $F_M/(chla \sigma_{PSII440})$ and $F_0/(chla \sigma_{PSII440})$. The gray bar plot shows irradiance ($\mu\text{mol photons m}^{-2} \text{s}^{-1}$) dynamics over the course of the day (times)

variation is therefore mainly linked to $\sigma_{PSII440}$ dynamics. For *P. australis*, the slight decrease observed after 2 pm for $Y(II)_{\max}$ was associated with a slight increase in $F_M/chla$, while $F_M/(chla \sigma_{PSII440})$ remained stable (Fig. 2f). Thus, the $Y(II)_{\max}$ variation can be attributed to the observed increase in $\sigma_{PSII440}$ (Fig. 1b).

Photosynthetic parameters

The photosynthetic efficiency of PSII electron transport (α ; $\mu\text{mol L}^{-1} \text{h}^{-1} (\mu\text{mol photons m}^{-2} \text{s}^{-1})^{-1}$) showed different trends between species and methods (Fig. 3). The α^{a*} values (Fig. 3a) were higher than the $\alpha(II)$ values (Fig. 3b) especially for *P. australis*.

For *T. pseudonana*, the values of α^{a*} were significantly lower after 2 pm than before (RM ANOVA $p < 0.001$; Holm–Sidak pairwise comparison), while values of $\alpha(II)$ did not differ (RM ANOVA; $p = 0.059$). For *S. marinoi*, α^{a*} and $\alpha(II)$ values remained stable throughout the day despite the weak yet significant variations observed at 2 pm, 7:30 pm, and 8:30 pm in both parameters (RM ANOVA, $p < 0.001$; Holm–Sidak pairwise comparison). For *P. australis*, high variability between replicates resulted in no significant differences for α^{a*} (RM ANOVA, $p = 0.195$) and $\alpha(II)$ (RM ANOVA, $p = 0.048$) values.

The maximum electron transport rate (ETR_{\max} ; $\text{mmol}^{-1} \text{mgchl}a^{-1} \text{h}^{-1}$) differed as a function of the method of calculation used (Fig. 4). The mean values ranged between 0.49 and 10.26 $\text{mmol}^{-1} \text{mgchl}a^{-1} \text{h}^{-1}$ for ETR_{\max}^{a*} (Fig. 4a) and between 0.45 and 1.39 $\text{mmol}^{-1} \text{mgchl}a^{-1} \text{h}^{-1}$ for $\text{ETR}(II)_{\max}$ (Fig. 4b). An increase in ETR_{\max} values was observed in each species at the beginning of the day until reaching a maximum, whose timing and value differed as a function of the method and species (Table 1). After this maximum value, a decrease in ETR_{\max} values was observed. Comparison between the two ETR_{\max} estimations showed higher values for ETR_{\max}^{a*} than for $\text{ETR}(II)_{\max}$. The discrepancy between the two ETR estimations is species dependent (Table 1); the weakest relationships were observed for *P. australis*, and the biggest differences between ETR values were observed for *P. australis* with, respectively, a maximum value of $\text{ETR}(II)_{\max}$ of 1.19 $\text{mmol}^{-1} \text{mgchl}a^{-1} \text{h}^{-1}$ and maximum value of ETR_{\max}^{a*} of 10.26 $\text{mmol}^{-1} \text{mgchl}a^{-1} \text{h}^{-1}$.

Electron requirements for carbon fixation ($\varphi_{e,C}$)

$\text{pchl}(E)$ values were plotted against $\text{ETR}(E)$ values and strong linear regressions were found (Fig. 5; $R^2 > 0.92$). Using $\text{ETR}(II)$, $\varphi_{e,C}^{\sigma}$ (not corrected) values ranged between 3.06 and 6.74 mol electrons molC^{-1} , while after spectral correction, $\varphi_{e,C}^{\sigma}$ (corrected) values ranged between 1.92 and 3.57 mol electrons molC^{-1} . Using ETR^{a*} , $\varphi_{e,C}^{a*}$ values ranged between 1.69 and 43.20 mol electrons molC^{-1} (Table 2). The $\varphi_{e,C}^{\sigma}$ values by comparing the three times of sampling did not significantly differ over the course of the day (Table 3). Conversely, the $\varphi_{e,C}^{a*}$ values did significantly differ for *T. pseudonana* and *P. australis*. $\varphi_{e,C}^{a*}$. Values of *T. pseudonana* showed significant variations between the three sampling time (H1, H2, and H3), while for *P. australis*, $\varphi_{e,C}^{a*}$ values of H1 significantly differ from H2 and H3 (Table 3).

Discussion

Physiological responses to the light regime

Variations in phytoplankton productivity and associated physiological responses are known to occur at short time scales (Falkowski 1984; Greene et al. 1994; MacIntyre and Cullen 1996; Jouenne et al. 2005; Lavaud 2007). For diatoms, the degree of variability in photosynthesis appears to be particularly pronounced and it is assumed that diel oscillation in photosynthesis are not clock-controlled but regulated by diel variations in environmental light (Prézélin 1992; Dimier et al. 2007, 2009; Lavaud et al. 2007; Key et al. 2010; Wu et al. 2012). In addition, diel variability in photosynthetic parameters could also be linked to the cell cycle stage as shown on the diatom *Cylindrotheca fusiformis* synchronized by using cell cycle inhibitors (Claquin et al. 2004), but here, the cell cycle influence is hidden because the diatom growth is not naturally synchronized (Martin-Jézéquel et al. 2000; Claquin et al. 2004). In this study, photosynthetic parameters showed no parallel changes with the irradiance level. Indeed, despite an increasing trend in photosynthetic parameters ($\text{ETR}(II)_{\max}$, α , $Y(II)_{\max}$) in the morning correlated with the irradiance level, the highest values were not correlated with the maximum intensity (Figs. 3, 4; Table 1). The relationship between light and photosynthesis is clearly described: at the lowest light levels, photosynthesis is a linear function of irradiance while with increasing light, photosynthesis becomes light-saturated and remains unchanged unless photoinhibition occurs, which leads to a decrease in photosynthetic capacity (Behrenfeld et al. 2004). In *T. pseudonana* and *S. marinoi*, the highest values in the morning were followed by decreasing values at the highest intensity. This result suggests activation of photoacclimation

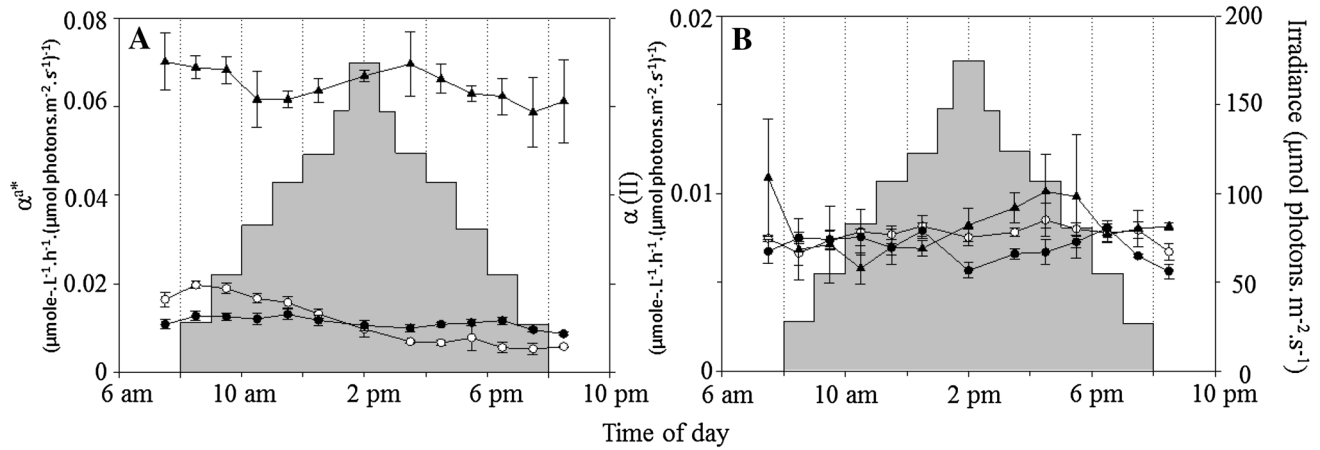


Fig. 3 Dynamics of the photosynthetic efficiency of the PSII (α ; rel. unit) calculated using **a** a^* (α^{a^*}) and **b** σ_{PSII440} ($\alpha(\text{II})$) for each species studied. The black circles represent *S. marinoi*, the white circles rep-

resent *T. pseudonana*, and the black triangles represent *P. australis*. The gray bar plot shows irradiance ($\mu\text{mol photons m}^{-2} \text{s}^{-1}$) dynamics over the course of the day (times)

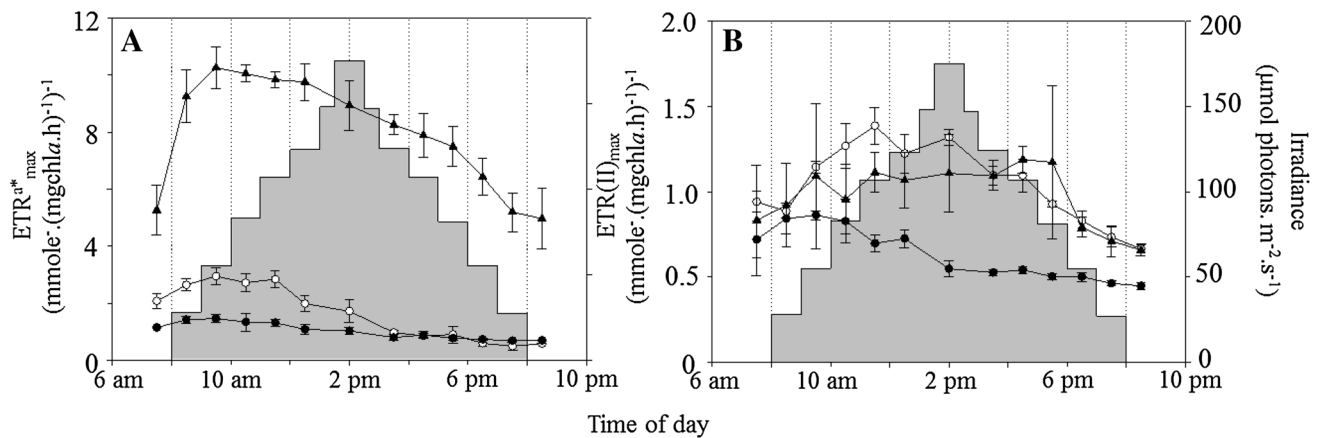


Fig. 4 Dynamics of the maximum electron transport rate (ETR_{max} ; relative unit) calculated using **a** a^* ($\text{ETR}^{a^*}_{\text{max}}$) and **b** σ_{PSII440} ($\text{ETR}(\text{II})_{\text{max}}$) for each species studied: *T. pseudonana* (empty circles);

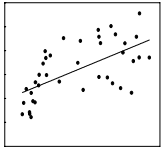
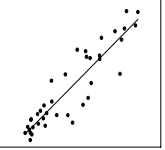
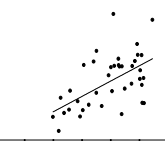
S. marinoi (black circles); and *P. australis* (black triangles). The gray bar plot shows irradiance ($\mu\text{mol photons m}^{-2} \text{s}^{-1}$) dynamics over the course of the day (times)

processes leading to reorganization and/or to reduction in pigment content under excessive light intensity to protect cells against possible damage to photosynthetic units, which can cause a slight decrease in photosynthetic efficiency (Macintyre et al. 2002; Dubinsky and Stambler 2009).

As samples were adapted to darkness before PAM measurements, any modulation of $Y(\text{II})_{\text{max}}$ values was caused by an increase in non-photochemical quenching (q_N) which may have two major explanations: (i) a reorganization of PSII antennae to increase the dissipation of energy or (ii) the alteration of photosystems corresponding to damage on PSII reaction centers (Kolber and Falkowski 1993). The first reason could thus be illustrated by the variation in functional absorption cross section of the PSII (σ_{PSII440}) values, while the second reason will be independent from it but will still influence F_V/F_M . As observed for *T. pseudonana* in this

study (Fig. 2), $Y(\text{II})_{\text{max}}$ dynamics was independent from σ_{PSII440} as illustrated by the decrease in $F_0/(\text{chl} a \sigma_{\text{PSII440}})$ in comparison with $F_0/\text{chl} a$. At 2 pm, the decrease in $Y(\text{II})_{\text{max}}$ is due to a decrease in $F_M/\text{chl} a$, while $F_0/\text{chl} a$ remains constant and can be explained by short-term photoacclimation as regulation of the xanthophyll cycle. After 2 pm, the decrease in $F_0/(\text{chl} a \sigma_{\text{PSII440}})$ which represents a proxy for the concentration of active reaction centers (Oxborough et al. 2012) could illustrate some damage in the photosystems. However, due to the relatively low irradiance applied ($175 \mu\text{mol photons m}^{-2} \text{s}^{-1}$), this hypothesis is debatable and the decrease observed in $F_0/(\text{chl} a \sigma_{\text{PSII440}})$ could rather be induced by some other photoacclimation processes which could induce a decrease in the concentration of active PSII and thus a decrease of the PSII to PSI ratio. In *S. marinoi*, $Y(\text{II})_{\text{max}}$ dynamics were linked to σ_{PSII440} values and thus could be

Table 1 Linear regression and Spearman correlation between the two ETR estimations using a^* ($\text{ETR}^{a^*}_{\text{max}}$) and σ_{PSII440} ($\text{ETR}(\text{II})_{\text{max}}$) for each species studied

<i>T. pseudonana</i>	<p>Maximum $\text{ETR}^{a^*}_{\text{max}}$ = 2.94 $\text{mmole}^{-1}\cdot\text{mgchl}a^{-1}\cdot\text{h}^{-1}$; recording time: 9:30 am Maximum $\text{ETR}(\text{II})_{\text{max}}$ = 1.39 $\text{mmole}^{-1}\cdot\text{mgchl}a^{-1}\cdot\text{h}^{-1}$; recording time: 11:30 am Linear regression: $\text{ETR}(\text{II})_{\text{max}} = 0.37 + 0.07 \times \text{ETR}^{a^*}_{\text{max}}$ $R^2 = 0.39$; p-value < 0.01; n=39 Spearman correlation coefficient: 0.65 p-value < 0.001; n = 39</p>	
<i>S. marinoi</i>	<p>Maximum $\text{ETR}^{a^*}_{\text{max}}$ = 1.46 $\text{mmole}^{-1}\cdot\text{mgchl}a^{-1}\cdot\text{h}^{-1}$; recording time: 9:30 am Maximum $\text{ETR}(\text{II})_{\text{max}}$ = 0.86 $\text{mmole}^{-1}\cdot\text{mgchl}a^{-1}\cdot\text{h}^{-1}$; recording time: 9:30 am Linear regression: $\text{ETR}(\text{II})_{\text{max}} = 0.15 + 0.15 \times \text{ETR}^{a^*}_{\text{max}}$ $R^2 = 0.84$; p-value < 0.001; n=39 Spearman correlation coefficient: 0.91 p-value > 0.05; n = 39</p>	
<i>P. australis</i>	<p>Maximum $\text{ETR}^{a^*}_{\text{max}}$ = 10.26 $\text{mmole}^{-1}\cdot\text{mgchl}a^{-1}\cdot\text{h}^{-1}$; recording time: 9:30 am Maximum $\text{ETR}(\text{II})_{\text{max}}$ = 1.19 $\text{mmole}^{-1}\cdot\text{mgchl}a^{-1}\cdot\text{h}^{-1}$; recording time: 5:30 pm Linear regression: $\text{ETR}(\text{II})_{\text{max}} = 0.79 + 0.15 \times \text{ETR}^{a^*}_{\text{max}}$ $R^2 = 0.15$; p-value < 0.001; n=39 Spearman correlation coefficient: 0.48 p-value < 0.01; n = 39</p>	

The correlation coefficient, the p value and the headcount (n) are given for each analysis. The maximum values of each ETR are given with the recording time. The plot represents the $\text{ETR}(\text{II})_{\text{max}}$ values (Y axis) as a function of the $\text{ETR}^{a^*}_{\text{max}}$ values (X axis) fitted to the linear regression whose equation is given

explained by reorganization of the PSII antennas. This observation is in agreement with the work of Weis and Berry (1987) who showed that an increase in q_N could be induced by a decrease in σ_{PSII} . In *P. australis*, $\text{ETR}(\text{II})_{\text{max}}$ remained constant when the light levels were high. A decrease in light absorption illustrated by a^* values was offset by an increase in σ_{PSII440} values which appears to allow constant electron transport inside the PSII. Thus, the diatom species investigated in this study appear to have regulated their absorption of energy used for photosynthesis by activation of physiological responses, such as the modulation of σ_{PSII440} to optimize photosynthesis like *P. australis* or to prevent damage to PSII like *S. marinoi*. These results confirm the species-dependent capacities and the different strategies used for photoacclimation in the same phylum.

Dynamics of $\varphi_{e,C}$

In this study, rETR values were used to estimate ETR using two commonly used methods, ETR^{a^*} (Barranguet and Kromkamp 2000; Morris and Kromkamp 2003; Napoléon and Claquin 2012; Napoléon et al. 2013b) and $\text{ETR}(\text{II})$ (Schreiber et al. 2012). ETR^{a^*} values were higher than $\text{ETR}(\text{II})$ and the ETR_{max} obtained using the two methods were weakly correlated (Table 1). This result can be easily explained as due to a^* estimation which corresponds to an average of total pigment absorption including non-photosynthetic and photo-protective pigments but also including a “package effect” (Fujiki and Taguchi 2002; Johnsen

and Sakshaug 2007) which can vary with the length and the biovolume of the species. This is in accordance with our data. *S. marinoi* which present the lowest biovolume of tested species showed the highest correlation between both ETR_{max} . However, $\text{ETR}(\text{II})$ is based on σ_{PSII} measurements at a narrow waveband (440 nm in the present study) which does not represent the whole photosynthetic active radiation spectrum (Schreiber et al. 2012). Thus, both approaches present some biases which can lead to a weak correlations between the two ETR estimates as a function of pigment phytoplankton groups (Johnsen and Sakshaug 2007), growth conditions (Hancke et al. 2008a; Napoléon et al. 2013b), and species (present study). Here, the two approaches were used to evaluate the discrepancy between $\varphi_{e,C}$ estimations and to assess the impact of the method on the characterization of $\varphi_{e,C}$ daily dynamics. In the three species studied, a linear relationship was obtained between ETR and P^{chl} values in agreement with the results of previous studies (Lawrenz et al. 2013; Napoléon et al. 2013b), which confirms that it is possible to accurately estimate primary productivity using variable fluorescence measurements (Barranguet and Kromkamp 2000; Napoléon and Claquin 2012). Our results showed that the method used influences greatly the $\varphi_{e,C}$ estimations and it is consequently important to consider which method was used before comparing studies or $\varphi_{e,C}$ estimations in different locations and conditions.

Considerable spatial and temporal variability of $\varphi_{e,C}$ values is reported in the literature (Lawrenz et al. 2013; Napoléon and Claquin 2012; Hancke et al. 2015). At longer

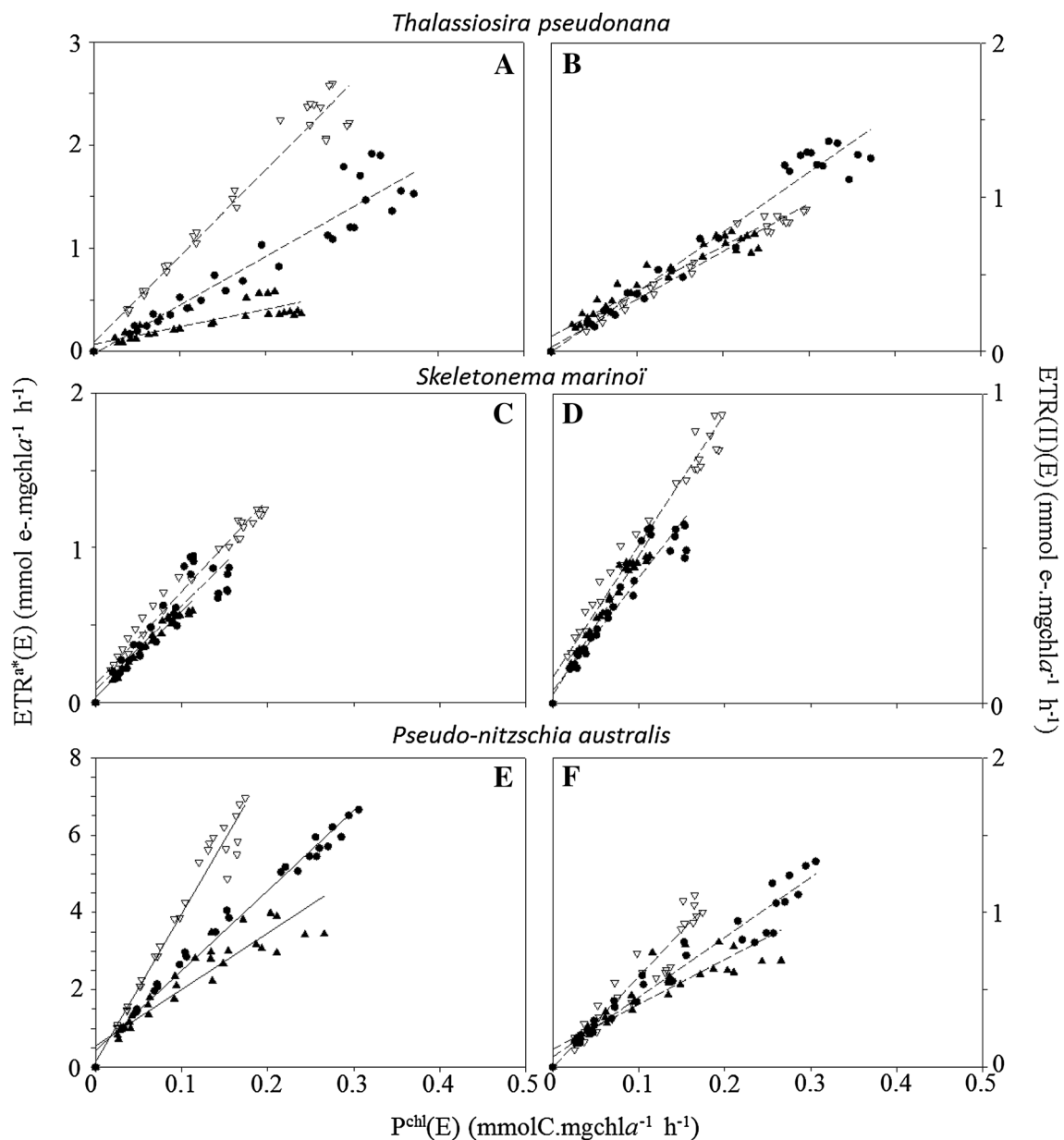


Fig. 5 Linear relationship between $ETR(E)$ ($ETR(II)$ or ETR^{a*} ; $mmol^{-} mgChla^{-1} h^{-1}$) and $P^{chl}(E)$ ($mmolC mgChla^{-1} h^{-1}$) for each species studied: (*T. pseudonana* (a, b), *S. marinoi* (c, d), and *P. aus-*

tralis (e, f) at each sampling time (9:30 am: white triangle; 2:00 pm: black circles; 7:30 pm: black triangles)

time scales, it is accepted that $\varphi_{e,C}$ variability is influenced by the seasonal dynamics of environmental parameters (light, nutrients, temperature, etc.) and by the species composition of phytoplankton assemblages. At the daily scale, our results showed that variability of $\varphi_{e,C}$ from ETR^{a*} can be higher between triplicates at the same sampling time than at the different sampling time over the course of the day, as shown by the high standard deviations for *S. marinoi* (Table 2). Thus, daily estimation of the primary production using the ETR^{a*} will have to take into consideration the large variability and the weak repetitiveness in the resulting

values. The variation in $\varphi_{e,C}^{\sigma}$ values estimated using $ETR(II)$ presented a lower variability over the course of the day with notable repetition between replicates (Table 2). For the estimation of daily primary production, it therefore appears that the $\varphi_{e,C}^{\sigma}$ values are better suited to transforming variable fluorescence data into carbon rate units without needing to take any daily variations into consideration. This result means it could be possible to estimate high-frequency primary production using autonomous variable fluorescence measurements from ships-of-opportunity or moorings (Napoléon and Claquin 2012; Lawrenz et al. 2013; Silsbe et al. 2015;

Table 2 Hourly and daily $\varphi_{e,C}$ values (mean \pm SD) estimated from the linear regressions ($y = ax + b$) between ETR(E) (mmol mgChl a^{-1} h $^{-1}$) and Pchl(E) (mmolC mgChl a^{-1} h $^{-1}$) for each species studied (three replicates per species)

Species	Time of day	P^{chl} vs. ETR a*		P^{chl} vs. ETR(II)			
		$\varphi_{e,C}^{a*}$	R^2	$\varphi_{e,C}^{\sigma}$ not corrected	R^2	$a^{*440}:a^{*}$	$\varphi_{e,C}^{\sigma}$ corrected
<i>T. pseudonana</i>	8:30 am	8.85 \pm 1.0	0.99	3.24 \pm 0.21	0.99	1.68	1.92 \pm 0.11
	2 pm	4.64 \pm 0.95	0.99	3.93 \pm 0.45	0.99	1.66	2.37 \pm 0.27
	7:30 pm	2.16 \pm 0.74	0.96	3.52 \pm 0.47	0.96	1.58	2.22 \pm 0.29
	Daily	5.21 \pm 3.03	–	3.56 \pm 0.45	–	–	2.17 \pm 0.22
<i>S. marinoi</i>	8:30 am	6.80 \pm 0.07	0.98	4.85 \pm 0.21	0.98	1.88	2.58 \pm 0.11
	2 pm	6.44 \pm 1.64	0.98	4.12 \pm 0.70	0.98	1.85	2.23 \pm 0.38
	7:30 pm	6.04 \pm 0.39	0.99	4.91 \pm 0.39	0.99	1.92	2.56 \pm 0.20
	Daily	6.43 \pm 0.91	–	4.62 \pm 0.56	–	–	2.45 \pm 0.23
<i>P. australis</i>	8:30 am	39.74 \pm 4.02	0.99	5.77 \pm 1.01	0.99	1.62	3.57 \pm 0.62
	2 pm	22.63 \pm 0.37	0.99	4.12 \pm 0.50	0.99	1.61	2.56 \pm 0.31
	7:30 pm	18.19 \pm 2.92	0.92	3.69 \pm 0.74	0.92	1.64	2.25 \pm 0.45
	Daily	26.86 \pm 10.17	–	4.53 \pm 1.16	–	–	2.79 \pm 0.46

With $y = \text{ETR(E)}$ (ETR(II) or ETRa^*), $x = \text{Pchl(E)}$, and R^2 the correlation coefficient of the relationship all replicates pooled. The spectral correction was applied on the $\varphi_{e,C}$ values from ETR(II) using the ratio $a^{*440}:a^*$

Table 3 Results of the one way repeated measures analysis of variance (RM ANOVA) for the $\varphi_{e,C}$ values which were estimated from the linear regressions between ETR(E) (ETR(II) or ETRa^*) and Pchl(E) for each species studied (three replicates per species)

Species	$\varphi_{e,C}^{a*}$		$\varphi_{e,C}^{\sigma}$	
	p value	Holm–Sidak method	p value	Holm–Sidak method
<i>T. pseudonana</i>	<0.001	H1 ^a –H2 ^b –H3 ^c	0.237	Not significant
<i>S. marinoi</i>	0.713	Not significant	0.228	Not significant
<i>P. australis</i>	<0.001	H1 ^a –H2 ^b –H3 ^b	0.102	Not significant

The difference was considered as significant when p value < 0.05. If difference was significant, an all pairwise multiple comparison procedure was performed using the Holm–Sidak method. The differences between sampling times (H1, H2, or H3) are given by a group name (a , b , or c) in exponent

Houliet et al. 2017, Claquin et al. in prep) without taking a potential daily variation in $\varphi_{e,C}$ into consideration. However, in this work, cultures are grown in controlled environments which are far from in situ conditions encountered by phytoplankton communities like the potential nutrient deprivations or the biotic/abiotic stresses for instance. Therefore, further investigations are needed to validate our finding for field application. Anyway, low-frequency $\varphi_{e,C}$ estimations are still necessary as a function of water masses and seasons.

The $\varphi_{e,C}^{\sigma}$ values obtained in this study with ETR(II) , which ranged from 3.06 to 6.74 mol electron molC $^{-1}$ before spectral correction and ranged from 1.92 to 3.57 mol electron molC $^{-1}$ after spectral correction, were in the range defined in several studies referenced by Lawrenz et al. (2013) at between 1.15 and 54.2 mol electron molC $^{-1}$ with a mean of 10.9 mol electron molC $^{-1}$, and in the lower range to the values obtained from PAM measurements (Hancke et al. 2015 and citations therein). However, our values were low compared to a large number of $\varphi_{e,C}$.

estimated in situ which, for example, ranged between 15.9 and 35.7 mol electron molC $^{-1}$ for deep alpine lake phytoplankton (Kaiblinger and Dokulil 2006) or between 9.17 and 125 mol electron molC $^{-1}$ for nutrient-limited cultures of phytoplankton (Napoléon et al. 2013b). The primary sources of $\varphi_{e,C}$ variation are variations in environmental parameters which lead to high values of $\varphi_{e,C}$ including salinity, temperature (Morris and Kromkamp 2003), nutrient limitations (Babin et al. 1996), a shift in community composition, or light stress (Napoléon and Claquin 2012; Lawrenz et al. 2013). These results also confirm the low electron cost for diatoms to performing photosynthesis under non-limiting nutrient conditions (Napoléon et al. 2013b). Under optimal growth conditions, the value of $\varphi_{e,C}$ would be between 4 and 6 moles (Lawrenz et al. 2013) which is in agreement with the results obtained in the present study. Values of $\varphi_{e,C} < 4$ appear to be physically impossible and could be due to methodological or calculation errors that could lead to underestimations of

up to 53% (Lawrenz et al. 2013) but the present study was conducted under controlled conditions and methodological errors are thus assumed to be low. Moreover, with the spectral correction applied on the $\varphi_{e,C}^{\sigma}$ values that should lead to more accurate values, our results were systematically < 4 mol electron molC⁻¹. However, the $a^*_{PSII}:a^*$ ratios calculated to perform these corrections were overestimated because taking non-photosynthetic pigments as describe by Suggett et al. (2004) which lead to a slightly underestimation of the $\varphi_{e,C}^{\sigma}$ corrected values. The $a^*_{PSII}:a^*$ ratio values used as a correction factor were in agreement with the values described in the literature (Lawrenz et al. 2013 and citations therein); therefore, the bias of our correction is probably weak. Moreover, the ratio 435:675 nm (blue and red peaks of in vivo chl_a absorption spectra) which could give us an indication of the accessory pigment contribution did not differ between species (in mean 1.81 ± 0.38 for all species and sampling times). The low $\varphi_{e,C}^{\sigma}$ values observed suggest that an additional source of energy might be used for carbon fixation. It was recently shown that diatoms are able to optimize their photosynthesis through the exchange of energy between plastids and mitochondria (Bailleul et al. 2015). Indeed, when the ATP:NADPH ratio generated by a linear electron flow is insufficient to fuel CO₂ imports into the plastid and assimilation by the Calvin cycle, diatoms are able to produced additional ATP *via* alternative pathways, particularly through extensive energy exchanges between plastids and mitochondria. This process could explain our values of $\varphi_{e,C} < 4$ mol electron molC⁻¹ particularly since this activity has already been demonstrated in *T. pseudonana* (Bailleul et al. 2015). Further investigations are now needed to continue this work in order to improve our knowledge on electron fluxes related to carbon fixation and to improve future estimates of primary production estimated from these methods.

Acknowledgements We thank Juliette Fauchot and Bertrand Le Roy for providing the diatom strains and Anne-Flore Deton for technical assistance. We are also really grateful to Camille Napoleon for technical help and constructive exchanges during this study. This work was supported by the GIP Seine-Aval project "PROUESSE" and the SMILE 2 project supported by l'Agence de l'Eau Seine Normandie.

References

- Armbrust EV (2009) The life of diatoms in the world's oceans. *Nature* 459(7244):185–192
- Babin M, Morel A, Gagnon R (1994) An incubator designed for extensive and sensitive measurements phytoplankton photosynthetic parameters. *Limnol Oceanogr* 39(3):694–702
- Babin M, Morel A, Claustre H, Bricaud A, Kolber Z, Falkowski PG (1996) Nitrogen- and irradiance-dependent variations of the maximum quantum yield of carbon fixation in eutrophic, mesotrophic and oligotrophic marine systems. *Deep Sea Res* 43(8):1241–1272
- Bailleul B, Berne N, Murik O, Petroustos D, Prihoda J, Tanaka A et al (2015) Mitochondria drives CO₂ assimilation in diatoms. *Nature* 524:366–369
- Barranguet C, Kromkamp J (2000) Estimating primary production rates from photosynthetic electron transport in estuarine microphytobenthos. *Mar Ecol Prog Ser* 204:39–52
- Behrenfeld MJ, Prasil O, Babin M, Bruyant F (2004) in Search of a physiological basis for covariations in light-limited and light-saturated photosynthesis. *J Phycol* 40(1):4–25
- Buesseler KO (1998) The decoupling of production and particulate export in the surface ocean. *Glob Biogeochem Cycles* 12(2):297–310
- Claquin P, Kromkamp JC, Martin-Jezequel V (2004) Relationship between photosynthetic metabolism and cell cycle in a synchronized culture of the marine alga *Cylindrotheca fusiformis* (Bacillariophyceae). *Eur J Phycol* 39(1):33–41
- Claquin P, Probert I, Lefebvre S, Veron B (2008) Effects of temperature on photosynthetic parameters and TEP production in eight species of marine microalgae. *Aquat Microb Ecol* 51(1):1–11
- Cloern JE, Foster SQ, Kleckner a E (2014) Phytoplankton primary production in the world's estuarine-coastal ecosystems. *Biogeosciences* 11(9):2477–2501
- Dimier C, Corato F, Tramontano F, Brunet C (2007) Photoprotection and xanthophyll-cycle activity in three marine diatoms. *J Phycol* 43(5):937–947
- Dimier C, Giovanni S, Ferdinando T, Brunet C (2009) Comparative ecophysiology of the xanthophyll cycle in six marine phytoplanktonic species. *Protist* 160(3):397–411
- Dubinsky Z, Stambler N (2009) Photoacclimation processes in phytoplankton: mechanisms, consequences, and applications. *Aquat Microb Ecol* 56(2–3):163–176
- Dubinsky Z, Falkowski PG, Wyman K (1986) Light harvesting and utilization by phytoplankton. *Plant Cell Physiol* 27(7):1335–1349
- Ducklow HW, Steinberg DK, Buesseler KO (2001) Upper ocean carbon export and the biological pump. *Oceanography* 14(4):50–58
- Eilers PHC, Peeters JCH (1988) A model for the relationship between light intensity and the rate of photosynthesis in phytoplankton. *Ecol Model* 42(3–4):199–215
- Falkowski PG (1984) Physiological responses of phytoplankton to natural light regimes. *6(2):295–307*
- Fujiki T, Taguchi S (2002) Variability in chlorophyll a specific absorption coefficient in marine phytoplankton as a function of cell size and irradiance. *J Plankton Res* 24(9):859–874
- Geider RJ, Delucia EH, Falkowski PG, Finzi AC, Grime JP, Grace J et al. (2001) Primary productivity of planet earth: biological determinants and physical constraints in terrestrial and aquatic habitats. *Glob Change Biol* 7(8):849–882
- Gilbert M, Wilhelm C, Richter M (2000) Bio-optical modelling of oxygen evolution using in vivo fluorescence: comparison of measured and calculated photosynthesis/irradiance (P-I) curves in four representative phytoplankton species. *J Plant Physiol* 157(3):307–314. Available from: <http://linkinghub.elsevier.com/retrieve/pii/S0176161700800528>
- Greene RM, Kolber ZS, Swift DG, Tindale NW, Falkowski PG (1994) Physiological limitation of phytoplankton photosynthesis in the eastern equatorial pacific determined from variability in the quantum yield of fluorescence. *Limnol Oceanogr* 39(5):1061–1074
- Guillard RRL, Ryther JH (1962) Studies of marine planktonic diatoms: I. *Cyclotella nana* Hustedt, and *Detonula confervacea* (Cleve) Gran. *Can J Microbiol* 8(2):229–239
- Hama T, Miyazaki T, Ogawa Y, Iwakuma T, Takahashi M, Otsuki A et al (1983) Measurement of photosynthetic production of a

- marine phytoplankton population using a stable ^{13}C isotope. *Mar Biol* 73:31–36
- Hancke K, Hancke TB, Lasse M, Olsen LM, Johnsen G, Ronnie N (2008a) Temperature effects on microalgal photosynthesis-light responses measured by O_2 production, pulse-amplitude-modulated fluorescence, and ^{14}C assimilation. *J Phycol* 44:501–514
- Hancke K, Hancke TB, Olsen LM, Johnsen G, Glud RN (2008b) Temperature effects on microalgal photosynthesis-light responses measured by O_2 production, pulse-amplitude-modulated fluorescence and ^{14}C assimilation. 514:501–514
- Hancke K, Dalsgaard T, Sejr MK, Markager S, Glud RN (2015) Phytoplankton productivity in an arctic fjord (West Greenland): estimating electron requirements for carbon fixation and oxygen production. *PLoS ONE* 10(7):1–23
- Henson SA, Sanders R, Madsen E (2012) Global patterns in efficiency of particulate organic carbon export and transfer to the deep ocean. *Global Biogeochem Cycles* 26(1):1–14
- Houliet E, Simis S, Nenonen S, Ylöstalo P, Seppälä J (2017) Basin-scale spatio-temporal variability and control of phytoplankton photosynthesis in the Baltic Sea: the first multiwavelength fast repetition rate fluorescence study operated on a ship-of-opportunity. *J Mar Syst* 169:40–51
- Huisman J, Sharples J, Stroom JM, Visser PM, Kardinaal WEA, Verspagen J et al. (2004) Changes in turbulent mixing shift competition for light between phytoplankton species. 85(11):2960–2970
- Johnsen G, Sakshaug E (2007) Biooptical characteristics of PSII and PSI in 33 species (13 pigment groups) of marine phytoplankton, and the relevance for pulse-amplitude-modulated and fast-repetition-rate fluorometry 1. *J Phycol* 43(6):1236–1251
- Jouenne F, Lefebvre S, Véron B, Lagadeuc Y (2005) Biological and physicochemical factors controlling short-term variability in phytoplankton primary production and photosynthetic parameters in a macrotidal ecosystem (eastern English Channel). *Estuar Coast Shelf Sci* 65(3):421–439
- Juneau P, Harrison PJ (2005) Comparison by PAM fluorometry of photosynthetic activity of nine marine phytoplankton grown under identical conditions. *Photochem Photobiol* 81(3):649–653
- Kaiblinger C, Dokulil MT (2006) Application of fast repetition rate fluorometry to phytoplankton photosynthetic parameters in freshwaters. *Photosynth Res* 88(1):19–30
- Key T, McCarthy A, Campbell DA, Six C, Roy S, Finkel ZV (2010) Cell size trade-offs govern light exploitation strategies in marine phytoplankton. *Environ Microbiol* 12(1):95–104
- Kolber Z, Falkowski PG (1993) Use of active fluorescence to estimate phytoplankton photosynthesis in situ. *Limnol Oceanogr* 38(8):1646–1665
- Kromkamp JC, Forster RM (2003) The use of variable fluorescence measurements in aquatic ecosystems: differences between multiple and single turnover measuring protocols and suggested terminology. *Eur J Phycol* 38:103–112
- Lavaud J (2007) Fast regulation of photosynthesis in diatoms: mechanisms, evolution and ecophysiology [Internet]. Vol. 1, *Funct Plant Sci Biotechnol*. Available from: <https://hal.archives-ouvertes.fr/hal-01094678/>
- Lavaud J, Strzepek RF, Kroth PG (2007) Photoprotection capacity differs among diatoms: possible consequences on the spatial distribution of diatoms related to fluctuations in the underwater light climate. *Limnol Oceanogr* 52(3):1188–1194
- Lavergne J, Trissl HW (1995) Theory of fluorescence induction in photosystem II: derivation of analytical expressions in a model including exciton-radical-pair equilibrium and restricted energy transfer between photosynthetic units. *Biophys J* 68(6):2474–2492
- Lawrenz E, Silsbe G, Capuzzo E, Ylöstalo P, Forster RM, Simis SGH et al (2013) Predicting the electron requirement for carbon fixation in seas and oceans. *PLoS One* 8(3):e58137
- Litchman E (1998) Population and community responses of phytoplankton to fluctuating light. *Oecologia* 117:247–257
- MacIntyre H, Cullen J (1996) Primary production by suspended and benthic microalgae in a turbid estuary: time-scales of variability in San Antonio Bay, Texas. *Mar Ecol Prog Ser* 145(1–3):245–268
- Macintyre HL, Kana TM, Anning T, Geider RJ (2002) Review photoacclimation of photosynthesis irradiance response curves and photosynthetic pigments in microalgae and cyanobacteria. *J Phycol* 38:17–38
- Marchetti A, Juneau P, Whitney FA, Wong CS, Harrison PJ (2006) Phytoplankton processes during a mesoscale iron enrichment in the NE subarctic Pacific: part II-Nutrient utilization. *Deep Sea Res Part II* 53(20–22):2114–2130
- Martin-Jézéquel V, Hildebrand M, Brzezinski MA (2000) Silicon metabolism in diatoms: implications for growth. *J Phycol* 36(5):821–840. <https://doi.org/10.1046/j.1529-8817.2000.00019.x>
- Morris EP, Kromkamp JC (2003 May) Influence of temperature on the relationship between oxygen- and fluorescence-based estimates of photosynthetic parameters in a marine benthic diatom (*Cylindrotheca closterium*). *Eur J Phycol* 38(2):133–142
- Napoléon C, Claquin P (2012) Multi-parametric relationships between PAM measurements and carbon incorporation, an in situ approach. *PLoS ONE* 7(7):1–12
- Napoléon C, Fiant L, Raimbault V, Claquin P (2013a) Study of dynamics of phytoplankton and photosynthetic parameters using opportunity ships in the western English Channel. *J Mar Syst* 128:146–158
- Napoléon C, Raimbault V, Claquin P (2013b) Influence of Nutrient Stress on the relationships between PAM measurements and carbon incorporation in four phytoplankton species. *PLoS ONE* 8(6):e66423
- Nelson DM, Tréguer P, Brzezinski MA, Leynaert A, Quéguiner B (1995) Production and dissolution of biogenic silica in the ocean: revised global estimates, comparison with regional data and relationship to biogenic sedimentation. *Glob Biogeochem Cycle* 9:359–372
- Oxborough K, Moore CM, Suggett DJ, Lawson T, Chan HG, Geider RJ (2012) Direct estimation of functional PSII reaction center concentration and PSII electron flux on a volume basis: a new approach to the analysis of Fast Repetition Rate fluorometry (FRRf) data. *Limnol Oceanogr* 10:142–154
- Pauly D, Christensen V (1995) Primary production required to sustain global fisheries. 374(March):255–257
- Prézélin BB (1992) Diel periodicity in phytoplankton productivity. *Hydrobiologia* 238(1):1–35
- Schreiber U, Klughammer C, Kolbowski J (2012) Assessment of wavelength-dependent parameters of photosynthetic electron transport with a new type of multi-color PAM chlorophyll fluorometer. *Photosynth Res* 113(1–3):127–144
- Schuback N, Hoppe CJM, Tremblay J-É, Maldonado MT, Tortell PD (2017) Primary productivity and the coupling of photosynthetic electron transport and carbon fixation in the Arctic Ocean. *Limnol Oceanogr* 62(3):898–921
- Shibata K, Benson AA, Calvin M (1954) The absorption spectra of suspensions of living micro-organisms. *Biochim et Biophysica Acta* 15:461–470
- Silsbe GM, Oxborough K, Suggett DJ, Forster RM, Ihnken S, Komárek O et al (2015) Toward autonomous measurements of photosynthetic electron transport rates: an evaluation of active fluorescence-based measurements of photochemistry. *Limnol Oceanogr* 13(3):138–155
- Suggett DJ, MacIntyre HL, Geider RJ (2004) Evaluation of biophysical and optical determinations of light absorption by photosystem II in phytoplankton. *Limnol Oceanogr* 2:316–332
- Thorel M, Fauchot J, Morelle J, Raimbault V, Le Roy B, Miossec C et al (2014) Interactive effects of irradiance and temperature

- on growth and domoic acid production of the toxic diatom *Pseudo-nitzschia australis* (Bacillariophyceae). *Harmful Algae* 39:232–241
- Van De Poll WH, Janknegt PJ, Van Leeuwe MA, Visser RJW, Buma AGJ (2009) Excessive irradiance and antioxidant responses of an Antarctic marine diatom exposed to iron limitation and to dynamic irradiance. *J Photochem Photobiol B* 94(1):32–37
- Weis E, Berry JA (1987) Quantum efficiency of photosystem {II} in relation to “energy”-dependent quenching of chlorophyll fluorescence. *Biochim et Biophysica Acta* 894(2):198–208
- Welschmeyer NA (1994) Fluorometric analysis of chlorophyll a in the presence of chlorophyll b and pheopigments. *Limnol Oceanogr* 39(8):1985–1992
- Wu H, Roy S, Alami M, Green BR, Campbell DA (2012) Photosystem II photoinactivation, repair, and protection in marine centric diatoms. *Plant Physiol* 160(1):464–476
- Zhu Y, Ishizaka J, Tripathy SC, Wang S, Mino Y, Matsuno T et al (2016) Variation of the photosynthetic electron transfer rate and electron requirement for daily net carbon fixation in Ariake Bay, Japan. *J Oceanogr* 72(5):761–776